Mechanisms of selenium removal by partially oxidized magnetite nanoparticles for waste water remediation

Börsig, N.; Scheinost, A.; Schild, D.; Neumann, T.;

Originally published:

July 2021

Applied Geochemistry 132(2021), 105062

DOI: https://doi.org/10.1016/j.apgeochem.2021.105062

Perma-Link to Publication Repository of HZDR:

https://www.hzdr.de/publications/Publ-30871

MANUSCRIPT

Selenite and selenate adsorption mechanisms on partially oxidized magnetite nanoparticles

Nicolas Börsig [a,*], Andreas C. Scheinost [b,c], Dieter Schild [d], Thomas Neumann [e]

[a] Karlsruhe Institute of Technology (KIT), Institute of Applied Geosciences, Adenauerring 20b, 76131 Karlsruhe, Germany

[b] Helmholtz-Zentrum Dresden-Rossendorf (HZDR), Institute of Resource Ecology, Bautzner Landstraße 400, 01328 Dresden, Germany

[c] The Rossendorf Beamline (ROBL) at ESRF, 38043 Grenoble, France

[d] Karlsruhe Institute of Technology (KIT), Institute for Nuclear Waste Disposal, Hermann-von-Helmholtz-Platz 1, 76344 Eggenstein-Leopoldshafen, Germany

[e] Technische Universität Berlin, Institute of Applied Geosciences, Ernst-Reuter-Platz 1, 10587 Berlin, Germany

* Corresponding author: Tel.: +49 721 608-44878; nicolas.boersig@kit.edu (N. Börsig)

Keywords: selenium, oxyanions, Se(IV), Se(VI), iron oxides, maghemite, immobilization, retention, remediation, XPS, XAFS, XANES, EXAFS

Environmental Significance Statement (max. 120 words)

Affordable and easy-to-produce nanoparticles are widely used in wastewater treatment applications. The mixed-valence iron oxide mineral magnetite has emerged as suitable material for the remediation of contaminated wastewaters due to its magnetic properties and high reactivity. Since the physicochemical properties of magnetite are strongly influenced by oxidation, however, the retention behavior of nanoparticulate magnetite can change substantially in natural environments. In this study, we explore the retention efficiency and capacity of partially oxidized magnetite nanoparticles with respect to dissolved selenium oxyanions and illustrate the effective adsorption mechanisms. The obtained results significantly contribute to the understanding of the retention behavior of selenium oxyanions in contact with nanoparticulate magnetite/maghemite phases in oxic environments typical for waste water treatment.

Abstract

Magnetite nanoparticles are a promising cost-effective material for the remediation of polluted wastewaters. Due to their magnetic properties and their high adsorption and reduction potential, they are particularly suitable for the decontamination of oxyanion-forming contaminants, including the highly mobile selenium oxyanions selenite and selenate. However, little is known how in field applications the remediation efficiency of magnetite nanoparticles is affected by partial oxidation and the formation of magnetite/maghemite phases. Here we characterize the retention mechanisms and capacity of partially oxidized nanoparticulate magnetite for selenite and selenate at different pH conditions and ionic strengths. Selenate was retained only under acidic conditions and strongly influenced by competing chloride anions, indicative of outer-sphere adsorption. Although the adsorption of selenite was also adversely affected by increasing pH, substantial quantities were retained even at alkaline conditions. Using spectroscopic analyses (XPS, XAFS), both mononuclear edge-sharing (^{2}E) and binuclear corner-sharing (^{2}C) inner-sphere selenite surface complexes could be identified, while reduction to Se(0) or Se(-II) species could be excluded. Under favorable adsorption conditions up to pH ~8, the affinity of selenite to form ^{2}C surface complexes is higher, whereas at alkaline pH values and less favorable adsorption conditions ^{2}E complexes prevail. Our results demonstrate that magnetite can be used as a suitable reactant for the immobilization of selenium as selenite in remedial applications, even under oxic conditions and without the involvement of reduction processes.

Graphical abstract

This article provides new insights into the retention behavior of partially oxidized magnetite nanoparticles in contact with selenium oxyanions under oxic conditions

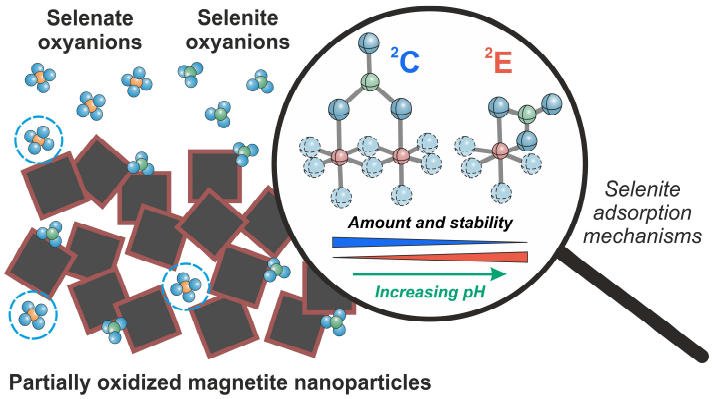

1 Introduction

Selenium (Se) pollution of soils, sediments and waters is a global phenomenon. Although Se is a naturally occurring trace element, the major cause of Se release and contamination are human activities such as coal production and combustion, phosphate and sulfide-ore mining, metal processing, oil refining, waste disposal or agricultural irrigation (Dhillon and Dhillon, 2003; Lemly, 2004; Tan et al., 2016). Additionally, Se occurs in vitrified high-level nuclear waste (HLW) in the form of the long-lived, harmful radionuclide ^{79}Se and plays a major role in the long-term safety assessment of HLW repositories (Frechou et al., 2007; De Cannière et al., 2010; Bingham et al., 2011).

In aquatic systems, Se levels can rapidly become toxic endangering not only the health of aquatic organisms but also of other beings, including humans, due to bioaccumulation in the food chain (Munier-Lamy et al., 2007; Lenz and Lens, 2009). Mobility and bioavailability of Se in water is mainly controlled by its solubility and retention through (bio)chemical processes (Dhillon and Dhillon, 2003; Fernández-Martínez and Charlet, 2009), which are largely determined by the prevailing Se oxidation state and related chemical speciation. Under reducing conditions, Se forms sparingly soluble minerals and compounds, primarily elemental selenium (Se^0) and metal selenides (Se(-I) and Se(-II)) (ESI Fig. A.1). Under (sub)oxic conditions, however, inorganic Se occurs in the oxidation state Se(IV) and Se(VI) as highly soluble and mobile oxyanions selenite (SeO_3^{2-}) and selenate (SeO_4^{2-}). Both selenite and selenate form protonated and deprotonated species depending on the solution pH (Fig. 1).

A key factor controlling the fate of dissolved Se oxyanions in aquatic environments is sorption on geological materials. Of special relevance in this context are metal (hydr)oxides and particularly iron (hydr)oxides due to their high affinity towards oxyanion-forming pollutants such as Se, As, Sb, V, Mo or Cr (Chan et al., 2009; Nakamaru and Altansuvd, 2014; Börsig et al., 2017; Weidner and Ciesielczyk, 2019). Besides adsorption, reduction of oxyanions to less soluble compounds is an important abiotic immobilization process (Wilkin et al., 2005; Kirsch et al., 2008; Scheinost et al., 2008), driven by Fe^0 or by Fe(II)-bearing iron (hydr)oxides, yet depends strongly on the prevailing redox conditions.

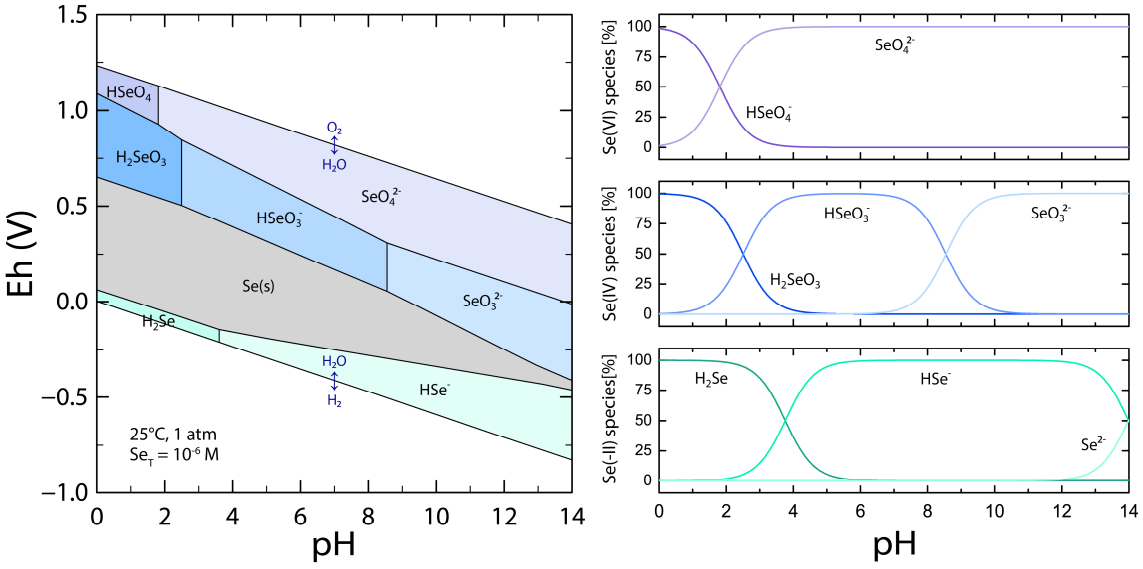

Fig. 1: (Left) Eh-pH diagram for the system Se-H_2O at 25°C and 1 atm; Se_{total}: 10^{-6} mol/L. (Right) Stability and distribution of dissolved Se(-II), Se(VI), and Se(VI) species as a function of pH. Diagrams were calculated with PHREEQC (USGS) using an adapted *wateq4f* database; thermodynamic Se data: aquatic species (Séby et al., 2001), solid phases (Salah and Wang, 2014).

Magnetite [Fe_3O_4] is one of the most widespread iron (hydr)oxide minerals in nature and is also known as a sink for dissolved oxyanions due to its high adsorption and reduction potential. Due to these properties and its magnetic character, which permits an easy separation of magnetite and associated contaminants from the waste water stream, the use of magnetite is considered in various in-situ and ex-situ environmental remediation approaches, including wastewater treatment or soil remediation (Kuppusamy et al., 2016; Usman et al., 2018). Particularly for decontamination of wastewaters based on the removal of hazardous oxyanions by nano-remediation, nanoparticulate magnetite is a promising cost-effective material (Chowdhury and Yanful, 2010; Horst et al., 2015; Li et al., 2017), as shown by several previous studies (Martínez et al., 2006; Scheinost and Charlet, 2008; Loyo et al., 2008; Jordan et al., 2009; Missana et al., 2009; Usman et al., 2018).

For field applications, however, it must be taken into account that reactivity and capacity of a remediation material is highly dependent on its stability under various environmental conditions. This applies in particularly for redox- and pH-sensitive minerals such as magnetite and other reduced or mixed-valent iron minerals like zerovalent iron (ZVI) and green rust (Génin et al., 2006; Liu et al., 2014; Mu et al., 2017; Börsig et al., 2018). A common phenomenon for magnetite is thereby the transformation into maghemite [γ-Fe_2O_3] under oxic conditions (ESI Fig. A.1) due to surface oxidation (Rebodos and Vikesland, 2010; Schwaminger et al., 2017).

$$2\ Fe^{II}Fe_2^{III}O_4 + 0.5\ O_2 \longrightarrow 3\ \gamma\text{-}Fe_2^{III}O_3$$

Maghemite is the Fe(II)-free oxidation product of magnetite and both minerals represent the end members of a solid solution series (Iwatsuki and Fukasawa, 1993; Gorski and Scherer, 2010). In case of larger magnetite crystals, oxidation of the mineral surface can result in the formation of a passivating layer of maghemite that protects the underlying magnetite from further oxidation (He and Traina, 2005; Rebodos and Vikesland, 2010; Khan et al., 2015). By contrast, magnetite nanoparticles produced by chemical synthesis usually consist of both magnetite and maghemite with a higher proportion of maghemite in the near-surface region (Kuhn et al., 2002; Signorini et al., 2003; Sharifi Dehsari et al., 2018).

In order to assess the efficiency of magnetite for remediation measures, it is therefore important to know to what extent oxidation and formation of a mixed magnetite/maghemite phase affects the retention of pollutants, particularly in terms of the specific mechanisms. The aim of this paper was therefore to characterize the retention efficiency of partially oxidized magnetite with respect to dissolved Se oxyanions. For this, we examined the interaction of selenite and selenate with pre-oxidized magnetite in adsorption experiments at various hydrochemical conditions, including pH and ionic strength. By using hydrochemical data and a combination of solids analysis, we were able to determine the Se retention capacity and stability as well as the involved immobilization mechanisms.

2 Materials and Methods

2.1 Synthesis of magnetite

Magnetite (Mt) was synthesized in the laboratory by progressively oxidizing an aquatic Fe^{2+} solution under alkaline pH conditions (ESI Fig. A.2). A detailed description of the synthesis procedure, the sample preparation as well as of the characterization of the final product can be found in Börsig et al. (2018). In short, 5 g $FeCl_2 \cdot 4\ H_2O$ were dissolved in 500 ml N_2-degassed Milli-Q water. After adding 55 mL 1 M KOH and 25 mL 1 M $NaHCO_3$ solution, blueish green colored iron(II) hydroxide precipitated. Continuous stirring resulted in the progressive oxidation of the initial anoxic system by atmospheric oxygen, causing the transformation of iron(II) hydroxide into black magnetite within 48 hours. With approximately 2 g of magnetite formed, the mass to volume ratio (m/V) during synthesis was about 3.4 g/L and the final pH was around 9.2. After synthesis, the magnetite phase was decanted, centrifuged and washed three times with Milli-Q water. After drying at 40°C, the synthesized particles were ground with an agate mortar and stored for analysis and adsorption experiments.

XRD analysis of the synthesis product proved the formation of magnetite [Fe_3O_4] without any indication of additional iron (hydr)oxide phases. According to SEM characterization, the magnetite consisted of aggregated particles with a single-particle size of about 50 nm. A specific surface area of 32 m²/g was determined by BET analysis, consistent with literature values (Cornell and Schwertmann, 2003; Salazar Camacho and Villalobos Peñalosa, 2017). XPS analysis and the evaluation of the Fe $2p_{3/2}$ spectra, however, showed that the Fe(II) to Fe_{total} ratio was only 0.14 (±5%) at the surface and therefore lower than the expected ratio of 0.33 for stoichiometric Fe_3O_4. Note that the information depth of the Fe $2p_{3/2}$ elemental line of magnetite was calculated with 2.2 nm (see ESI). This indicated that the synthesized magnetite was partially oxidized and that the near-surface region of these particles may consist of both magnetite and maghemite.

2.2 Adsorption experiments

Adsorption of selenite and selenate with this pre-oxidized magnetite was studied in batch experiments under oxic conditions. The experimental setup was almost identical to the conditions at the end of the magnetite synthesis. To investigate selenite and selenate adsorption as a function of the Se concentrations, 50 ml 0.01 M KCl solution that contained distinct volumes of Se stock solution was added to 170.0 mg of washed magnetite powder (m/V ratio = 3.4 g/L). The Se stock solutions were prepared by dissolving defined quantities of Na_2SeO_3 or $Na_2SeO_4 \cdot 10\ H_2O$ in N_2-degassed Milli-Q water. The added volumes were calculated to obtain initial selenite or selenate concentrations of 10^{-5} - 10^{-2} mol/L. KCl was used as background electrolyte since also the original synthesis took place in such conditions and to simulate solutions with higher ionic strengths. After mixing, the pH was adjusted to 9.2 by dropwise addition of KOH solution. The 50 mL flasks were sealed and shaken for 48 hours to ensure that adsorption equilibrium was achieved. Due to the strong buffer capacity of magnetite, pH was checked after 24 and 45 hours and if necessary readjusted to pH 9.2. Afterwards, the residual Se concentration in solution was analyzed and the solids were dried at 40°C both with and without prior washing.

In addition, similar batch experiments were carried out to study the influence of pH and ionic strength. While selenite or selenate concentration was kept constant (10^{-4} mol/L), different ionic strengths of 0.01 M KCl or 0.14 M KCl were tested and pH values were adjusted in the range of 2 to 14 using either HCl or KOH solution.

2.3 Analytical techniques

Dissolved Se and Fe concentrations were determined by Inductively-Coupled Plasma Optical Emission Spectrometry (ICP-OES; Varian 715ES) or Inductively-Coupled Plasma Mass Spectrometry (ICP-MS; X-Series 2, Thermo Fisher Scientific Inc.) depending on the solution concentrations. X-Ray Diffraction (XRD) for analysis of the mineral composition was performed on a Bruker D8 Advance X-ray diffractometer (Cu Kα). The total Se content of the solid phases was determined by polarized Energy Dispersive X-ray Fluorescence Spectroscopy (pEDXRF) with an Epsilon 5 (PANalytical). Electron microscopy with Energy Dispersive X-ray Spectroscopy (EDX) was used to characterize the solid phases. Images were recorded using a LEO 1530 (Zeiss Inc.) Scanning Electron Microscope (SEM) with a NORAN System SIX (Thermo Electron Corp.) EDX-System. To examine oxidation states and to identify elemental composition of the surface area, X-ray Photoelectron Spectroscopy (XPS) measurements were performed using a PHI 5000 VersaProbe II (ULVAC-PHI, Inc.). Detailed information about measurement parameters, sample preparation and data evaluation are described in the ESI.

X-ray absorption spectroscopy was carried out on selected samples to identify the Se oxidation state, coordination as well as the molecular short-range structure. Se K-edge X-ray Absorption Fine Structure (XAFS) spectra were collected at The Rossendorf Beamline (ROBL) at ESRF (Grenoble, France). Measurement parameters and sample preparation are described in detail in the ESI. Fluorescence deadtime correction, energy calibration and averaging of scans was performed with the software package SixPack {Webb, 2005 #609}(www.sams-xrays.com/sixpack), while normalization and extraction of the EXAFS chi function was performed with the software WinXAS according to standard procedures (Ressler, 1998). The k^3-weighted EXAFS data were fit using theoretical back-scattering amplitudes and phase shifts calculated with FEFF 8.2 (Ankudinov and Rehr, 1997). Statistical analysis of spectra was performed with the ITFA program package (Rossberg et al., 2003). Spectra of Se reference samples were taken from Scheinost and Charlet (2008).

3 Results and Discussion

3.1 Adsorption capacity of oxidized magnetite for selenite and selenate

Fig. 2a shows the adsorption capacity of magnetite for selenite and selenate under oxic conditions as a function of pH and ionic strength. The results demonstrate that the adsorption behavior is primarily affected by the Se species. Selenate is only immobilized under extreme acidic conditions, with about 50% of selenite adsorbed at pH 3. Contrary to selenate, the entire

initial selenite amount is immobilized at low pH (< pH 5) and the adsorption edge extends over a wide pH range from weakly acidic to alkaline (pH 6–11) conditions. Furthermore, while the adsorption edge of selenate shifts towards lower pH values (~1.5 pH unit) in the presence of higher KCl concentrations, retention of selenite is not affected by higher ionic strengths. Further confirmation for this observation can also be seen in Fig. 2b, which shows the distribution coefficient (K_d) as a function of the selenite equilibrium concentration at pH 9.2. With increasing concentrations of dissolved Se, log K_d values decrease steadily but are identical for both ionic strengths. The absolute K_d values are furthermore quite high (log K_d: 3.2–1.2 L/kg) and correspond to Se surface coverages in the range of 0.05 to 2.5 at/nm^2. Unlike selenite, the adsorption of selenate was too low to obtain reliable K_d data at pH 9.2.

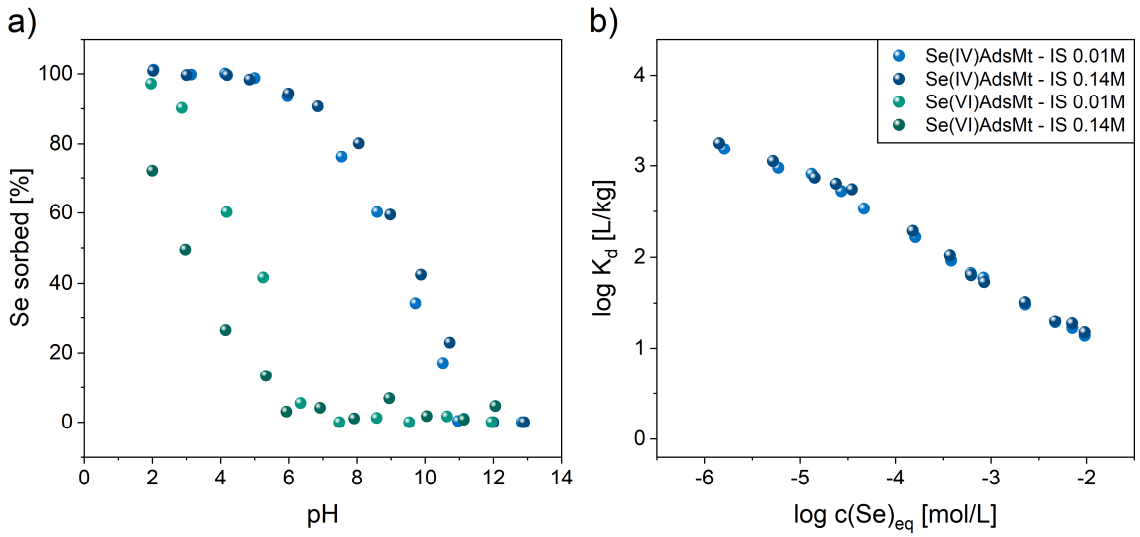

Fig. 2: (Left) Selenite and selenate adsorption on magnetite (Mt) depending on pH and ionic strength (IS) at initial Se concentrations of 10^{-4} mol/L. (Right) Uptake of selenite by magnetite at pH 9.2 as a function of the Se equilibrium concentration.

The observed adsorption behavior is consistent with the literature. Adsorption capacities of iron (hydr)oxides for anions such as selenite and selenate decrease with increasing pH as the amount of positively charged surface groups declines by deprotonation. Since in particular the single-protonated Se species ($HSeO_3^-$ and $HSeO_4^-$) interact with the hydroxyl groups on the magnetite surface (Martínez et al., 2006; Kim et al., 2012), the position of the adsorption edges also correlates with the pH-dependent distribution of those species in solution (Fig. 1). However, even at alkaline conditions of pH > 10, where the point of zero charge of magnetite (reported PZC values ranging from 6.5 to 8.1) is already exceeded and the surface is negatively charged (Milonjić et al., 1983; Hu et al., 2010), significant amounts of selenite are adsorbed. Responsible for this immobilization is the specific adsorption of selenite resulting in the

formation of inner-sphere surface complexes (Martínez et al., 2006; Loyo et al., 2008; Jordan et al., 2009; Kim et al., 2012). Due to this inner-sphere selenite adsorption, large distribution coefficients as well as high Se surface coverages of up to 2.5 at/nm^2 can be observed even at pH 9.2. Such values were found not only for magnetite (Kim et al., 2012) but also for hematite and goethite (Su and Suarez, 2000; Duc et al., 2003; Rovira et al., 2008; Börsig et al., 2017). In addition, formation of inner-sphere complexes explains why selenite adsorption is not dependent on the ionic strength. By contrast, selenate primarily forms outer-sphere adsorption complexes in contact with iron (hydr)oxides (Hayes et al., 1987; Rietra et al., 2001; Jordan et al., 2013). This would explain the almost non-existent adsorption at higher pH values as well as the negative impact of higher ionic strengths as both parameters cause unfavorable adsorption conditions due to decreasing positive surface charges and competition effects.

When interpreting these adsorption data, it must be taken into account that the used magnetite phase was partly oxidized to maghemite in its near-surface region under the prevailing oxic conditions. However, comparison of Se adsorption studies on magnetite and maghemite reveals that both minerals behave very much alike. The adsorption capacity of both maghemite and magnetite is similar in terms of its dependence on Se speciation, pH or ionic strength (Jordan et al., 2013; Jordan et al., 2014). Interesting is also that several previous Se adsorption studies on magnetite led to similar results regardless of whether the experiments were performed under oxic (Martínez et al., 2006) or anoxic conditions (Loyo et al., 2008; Jordan et al., 2009; Kim et al., 2012). In comparative studies Missana et al. (2009) proved that no differences in terms of selenite sorption occurred under oxic and anoxic conditions. Furthermore, it is not always documented to what extent the synthesized, industrially-produced or natural magnetite tested in the above mentioned sorption studies might also have been affected by a partial oxidation into maghemite. In contrast, magnetite synthesized under well controlled, anoxic conditions proved to be a very effective reducer for selenite {Scheinost, 2008 #139;Scheinost, 2008 #266}.

3.2 Effects of selenium adsorption on the properties of the solid phase

To assess the impact of selenite or selenate adsorption on the properties of the magnetite phase, selected samples from adsorption experiments were characterized by various solids analysis methods. A detailed description and evaluation of these analyses can be found in the ESI chapter 3.1. In short, XRD and SEM/EDX analyses demonstrated that neither the mineralogical composition (ESI Fig. A.3) nor the morphology (Fig. 3) of the initial magnetite nanoparticles was affected by the adsorption of selenite or selenate respectively. EDXRF data (ESI Table A.1) and SEM/EDX analysis (ESI Fig. A.4), however, proved that the examined solid samples

contained significant Se quantities after adsorption, whose proportions depend on the initial Se speciation and concentration. For a solid sample from the selenite system, with a relatively high total Se amount of 4,200 ppm, the oxidation state of this Se proportion was identified by XPS as Se(IV) (ESI Table A.2), demonstrating that the retention of selenite is not accompanied by a change of the Se oxidation state.

Furthermore, XPS analysis and the comparison of the Fe(II)/Fe_{total} ratio of the solids before and after the adsorption of selenite or selenate yielded to comparable results (ESI Table A.2). This observation that the oxidation of magnetite to maghemite is not progressing significantly during the oxic adsorption experiments, can be explained by the formation of an initial maghemite oxidation layer that prevents the underlying magnetite core from further aerial oxidation (He and Traina, 2005; Rebodos and Vikesland, 2010; Khan et al., 2015).

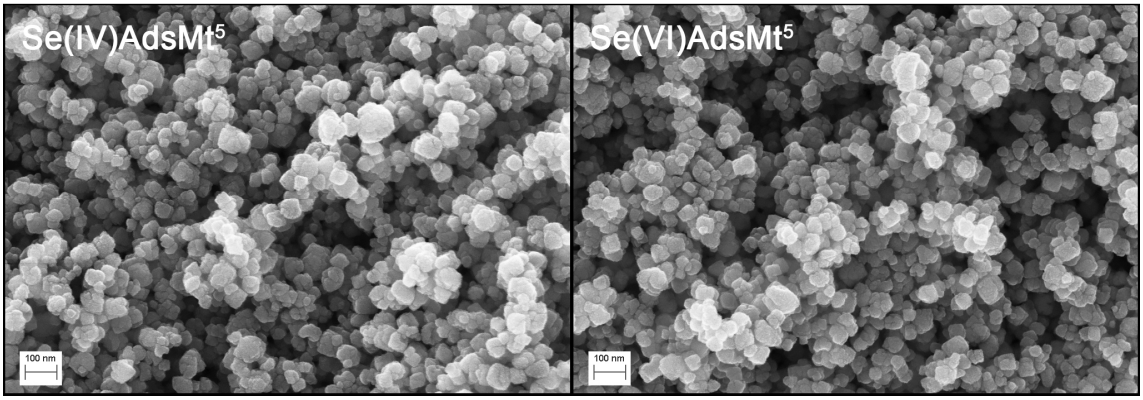

Fig. 3: SEM results of magnetite samples from selenite and selenate adsorption studies; $c(Se)_0 = 5 \times 10^{-3}$ mol/L.

3.3 Characterization of the adsorption complexes

Se K-edge XAFS analysis was used to characterize the oxidation state (XANES) as well as the local structure (EXAFS) of the immobilized Se. For this purpose, magnetite samples from selenite or selenate adsorption experiments conducted at pH 4, 7 and 9.2 were analyzed in order to investigate the influence of pH on the sorption mechanism.

Unfortunately, even at pH 4, selenate sorption on magnetite was too low to be analyzed by XAFS spectroscopy. A determination of the specific adsorption mechanisms was therefore not possible in case of the selenate system. However, the low retention capacity in combination with the negative impact of higher ionic strengths and pH values generally points to the formation of outer-sphere adsorption complexes. That selenate oxyanions form primarily outer-sphere complexes in contact to iron (hydr)oxides was previously shown for maghemite (Jordan

et al., 2013) and hematite (Börsig et al., 2017) by XAFS, as well as by SCM for magnetite (Martínez et al., 2006). It should be noted, however, that the observed dependency on ionic strength and pH alone is not an unambiguous characteristic in favor of an outer-sphere selenate adsorption (Su and Suarez, 2000).

Unlike the samples from the selenate systems, the selenite samples had taken up enough Se to be analyzed by XAFS analysis. Fig. 4 shows the Se K-edge XANES spectra of the analyzed samples from the selenite system together with reference spectra of Se(IV) (Na_2SeO_4 solution) and Se(0) (grey elemental Se) compounds. For all three samples, the adsorption edge exactly matches that of the Se(IV) reference spectra (12.660 KeV), indicating that the initial tetravalent oxidation state remained unchanged. XANES data are thus in line with the XPS results which showed that the adsorption processes caused neither selenite reduction nor oxidation. An immobilization due to selenite reduction and formation of sparingly soluble reduced Se compounds such as elemental Se^0 or selenide minerals can therefore be excluded not only at alkaline but also at acidic pH conditions. It is known that in anoxic systems reduction of selenite oxyanions by Fe(II)-bearing minerals like magnetite is generally possible (Scheinost et al., 2008; Scheinost and Charlet, 2008; Börsig et al., 2018). However, even in an anoxic environment, selenite reduction does not inevitably take place, as other selenite-magnetite adsorption studies have proven (Loyo et al., 2008; Jordan et al., 2009; Missana et al., 2009). The exact reasons for this are unclear, but several possible explanations have been discussed in previous studies. According to Loyo et al. (2008), one reason could be the slow reaction time of the selenite reduction process. However, a direct comparison of the reaction times used in the above mentioned studies, ranging from a few hours to 30 days, is difficult because of the partially very different experimental setups (i.e. initial Se concentrations, magnetite amounts, pH, presence of secondary ions, etc.). For this reason, the reaction time must rather be seen in relation to the respective mineral surface coverage and reduction kinetics. According to Missana et al. (2009), reduction of selenite oxyanions is only possible if the selenite surface coverage of the corresponding Fe(II)-bearing mineral phase is relatively low, as high coverages slow down electron transfer processes. This theory, however, has not yet been experimentally proven. Furthermore, the presence or absence of Se reduction processes could be affected by the specific Fe(II)/Fe(III) ratio of the magnetite phase, since the magnetite stoichiometry strongly influences its physicochemical properties, including the sorption capacity and the reduction potential (Gorski and Scherer, 2010). Higher Fe(II) fractions have a positive impact on the reduction potential of magnetite, which was proven in sorption studies with uranium (Latta et al., 2012) and neptunium (Wylie et al., 2016), among others.

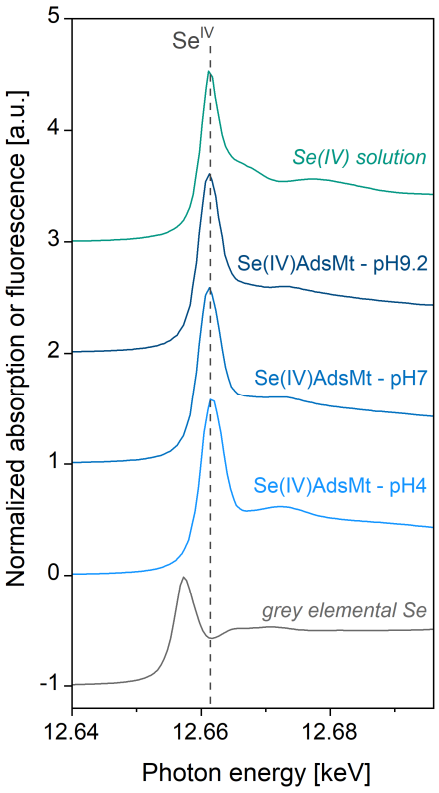

Fig. 4: Se K-edge XANES spectra of Se references and magnetite samples from selenite adsorption studies performed at different pH values; $c(Se)_0 = 10^{-3}$ mol/L.

To identify the specific adsorption type, the samples were analyzed by Se K-edge EXAFS spectroscopy (Fig. 4). The k^3-weighted spectra were fit with a FEFF 8.2 file generated with the crystallographic structure of mandarinoite ($Fe_2(SeO_3)_3 \cdot 6H_2O$, CIF 0005198, Hawthorne, 1984). For all three selenite sorption samples, the EXAFS Fourier transforms (FT) are dominated by a strong peak at 1.35 Å (uncorrected for phase shift). Responsible for this peak is the oxygen coordination shell. The fit of this shell using a single scattering Se-O path resulted in coordination number (CN) of 2.8 and atomic distances of 1.70–1.71 Å (Table 1), confirming the tetravalent oxidation state and the unchanged pyramidal-shaped molecular structure of the selenite oxyanion. Beyond the oxygen coordination shell, a small double peak arises in the range 2.3–3.5 Å (uncorrected for phase shift), with the relative ratio of the two peaks changing with pH: For the sample representing acidic conditions [Se(IV)AdsMt-pH4], the right-side peak at 2.9 Å dominates, whereas under alkaline conditions [Se(IV)AdsMt-pH9.2] the left-side peak at 2.6 Å becomes more pronounced. In addition, the peak intensities at alkaline pH are generally lower than for acidic conditions. The peaks could be fitted with two individual single scattering Se-Fe paths, providing between 0.3–0.9 Fe atoms at an atomic distance of 2.90–2.93 Å, and

0.4–0.9 Fe atoms at an atomic distance of 3.37–3.40 Å (Table 1). Note that the Debye-Waller factors of both Se-Fe paths were kept correlated, to achieve a satisfying fitting of those peaks. The graphical representation of the fit results can be found in ESI Fig. A.5.

Table 1: Se-K XANES edge energies and EXAFS fit results of selenite-magnetite adsorption samples (S_0^2 = 0.9).

		Oxygen shell				Iron shells						
Sample	**E_0 [keV]**	**CN[a]**		**R [Å][b]**	**σ² [Å²][c]**	**CN**		**R [Å]**	**σ² [Å²]**		**ΔE_0 [eV]**	**χ_{res} [%]**
Se(IV)AdsMt-pH4	12.6600	0.9	O	2.8	1.70	0.9	Fe	2.93	0.0093	[d]	14.8	12.5
						1.7	Fe	3.40	0.0093	[d]		
Se(IV)AdsMt-pH7	12.6595	0.9	O	2.8	1.70	0.5	Fe	2.93	0.0048	[d]	15.4	13.4
						0.6	Fe	3.39	0.0048	[d]		
Se(IV)AdsMt-pH9	12.6596	0.9	O	2.8	1.71	0.3	Fe	2.90	0.0030	[d]	15.7	14.6
						0.4	Fe	3.37	0.0030	[d]		

[a] CN: coordination number, error ± 25%. [b] R: radial distance, error ± 0.01 Å. [c] σ²: Debye-Waller factor, error ± 0.0005 Å². [d] correlated σ².

Although the necessity for such relatively small coordination numbers may be questioned at first due to their inevitably larger error, the use of two scattering paths was required to achieve stable fitting results. Contrary to this, the use of only one Se-Fe path or a mixture of Se-Fe and Se-O paths led to poor fitting results. Furthermore, data of other studies (Missana et al., 2009; Jordan et al., 2014) as well as the results of principal component analysis (see chapter 3.4) support this assumption.

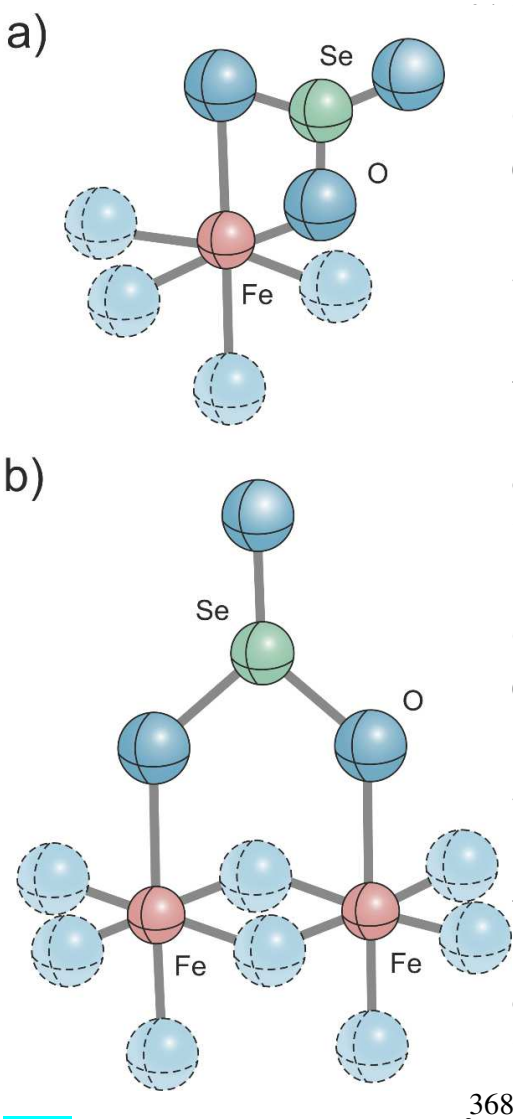

Fig. 5: Model showing the structure of (a) ^{2}E and (b) ^{2}C adsorption complexes between selenite molecules and FeO_6 octahedra.

The occurrence of Fe atoms in the second shell indicate an inner-sphere bonding between the selenite oxyanion and the mineral surface. The shorter Fe shell with a distance of 2.90–2.93 Å points to the formation of a bidentate mononuclear edge-sharing ^{2}E arrangement. As shown in Fig. 5a, ^{2}E adsorption complexes are characterized by two oxygen atoms of the selenite molecule simultaneously forming the edge of an FeO_6 octahedron on the iron (hydr)oxide surface. The longer Fe shell, on the other hand, represents bidentate binuclear corner-sharing ^{2}C adsorption complexes, where one adsorbed selenite molecule is attached to two FeO_6 octahedra (Fig. 5b). That the interaction of selenite oxyanions with iron (hydr)oxides can cause the (simultaneous) formation of these types of inner-sphere adsorption complexes, was also demonstrated by several previous studies (Hayes et al., 1987; Manceau and Charlet, 1994; Hiemstra et al., 2007; Missana et al., 2009; Jordan et al., 2014; Börsig et al., 2017).

According to the EXAFS results, other types of sorption or retention mechanisms can be excluded. For instance, Missana et al. (2009) reported formation of a discrete ferric selenite phase like $Fe_2(SeO_3)_3 \cdot 6H_2O$ at pH 4. This would results in higher Fe coordination numbers as well as in the presence of additional Se backscatter atoms, which are both missing in our EXAFS data. Also the formation of monodentate mononuclear corner-sharing ^{1}V complexes, which can arise for instance during the adsorption of As-oxyanions (arsenate or arsenite) on magnetite or maghemite can be ruled out (Morin et al., 2008; Zhang et al., 2011; Navarathna et al., 2019), since structural features in the EXAFS FT range beyond 3.5 Å are absent. Furthermore, we could exclude the presence of tridentate hexanuclear corner-sharing ^{3}C complexes, that have been shown to form with the oxyanions arsenite (Wang et al., 2008; Liu et al., 2015) and antimonite (Kirsch et al., 2008) at the {111} faces of magnetite, since

backscatterer atoms at higher atomic distances are absent. This assumption is supported by results of previous studies, in which also no hints for selenite ^{1}V or ^{3}C adsorption complexes on magnetite or maghemite have been found (Missana et al., 2009; Jordan et al., 2014). Jordan et al. (2014) explain this different behavior of selenite compared to arsenite or antimonite by the different sizes of these trigonal pyramidal oxyanion molecules.

3.4 Properties and stability of the selenite surface complexes

Based on XAFS data, interaction of dissolved selenite with magnetite under oxic conditions leads to the simultaneous formation of ^{2}E and ^{2}C adsorption complexes. Which types of adsorption complexes develop on a particular material generally depends on the prevailing hydrochemical conditions and the structural and morphological properties of the adsorbent phase. This can be explained by the atomic structure and features of specific crystal surfaces. Due to the distinct arrangement of functional surface groups or, respectively, adsorption sites, certain types of adsorption complexes occur mainly on certain crystal surfaces. Since the affinity of an adsorbate for certain adsorption sites is determined among other things by its general surface coverage (Peak and Sparks, 2002; Fukushi and Sverjensky, 2007), which in turn is influenced by the pH value, different crystal surfaces show different reactivities depending on the degree of coverage or pH. In case of oxyanion adsorption on magnetite, formation of ^{2}C adsorption complexes is mainly associated with the {100} crystal surface, while the ^{2}E complexes are related to the {110} or {111} facets (Jönsson and Sherman, 2008; Wang et al., 2008; Wang et al., 2011; Liu et al., 2015; Navarathna et al., 2019).

Changing selenite adsorption types depending on the solution pH were determined by EXAFS analysis for both magnetite (Missana et al., 2009) and maghemite (Jordan et al., 2014). The respective results indicate that ^{2}E and ^{2}C selenite adsorption complexes appear simultaneously at acidic conditions or at high surface coverages, respectively, with the corner-sharing ^{2}C complexes being dominant. With increasing pH values or decreasing surface coverages, the share of ^{2}C complexes tends to decrease and at alkaline conditions (>pH 8) only edge-sharing ^{2}E adsorption complexes occur. However, the authors of both studies noted that the evaluation of EXAFS data for such samples is quite difficult. Due to the small coordination numbers, especially at neutral or alkaline conditions, identification of the adsorption complexes as well as determination of their relative shares becomes more and more challenging. This challenge also arises for the EXAFS data of this work. Particularly the samples at pH 7 and pH 9.2 are characterized by small Fe coordination numbers, which makes it difficult to estimate their relative fractions.

We therefore performed a statistical analysis of the EXAFS spectra with Iterative Transformation Factor Analysis (ITFA) (Rossberg et al., 2003). ITFA allows determining the number of principal components (PC) and their respective factor loadings. Fig. 6a illustrates the good match between the experimental spectra (black) and their reconstructions (red lines) by two PC. The ITFA thus confirms that two individual spectral components are needed to characterize the EXAFS spectra of all three adsorption samples.

Moreover, the corresponding Varimax factor loadings (Fig. 6b) show that the sample at pH 4 is solely dominated by PC 1, whereas PC 2 primarily represents selenite adsorption under alkaline conditions. Based on the previous observations and the findings of Missana et al. (2009) and Jordan et al. (2014), these results can be interpreted in a way that the different factor loadings are associated with a varying distribution of ^{2}E and ^{2}C surface adsorption complexes. Accordingly, PC 1 reflects a combination of ^{2}E and ^{2}C adsorption complexes with a higher proportion of corner-sharing ^{2}C complexes, while PC 2 represents a mixture of both complexation types with a higher share of ^{2}E complexes. Under neutral or slightly alkaline conditions, both adsorption types would thus occur in approximately equal proportions, which is consistent with the factor loading of sample Se(IV)AdsMt-pH7.

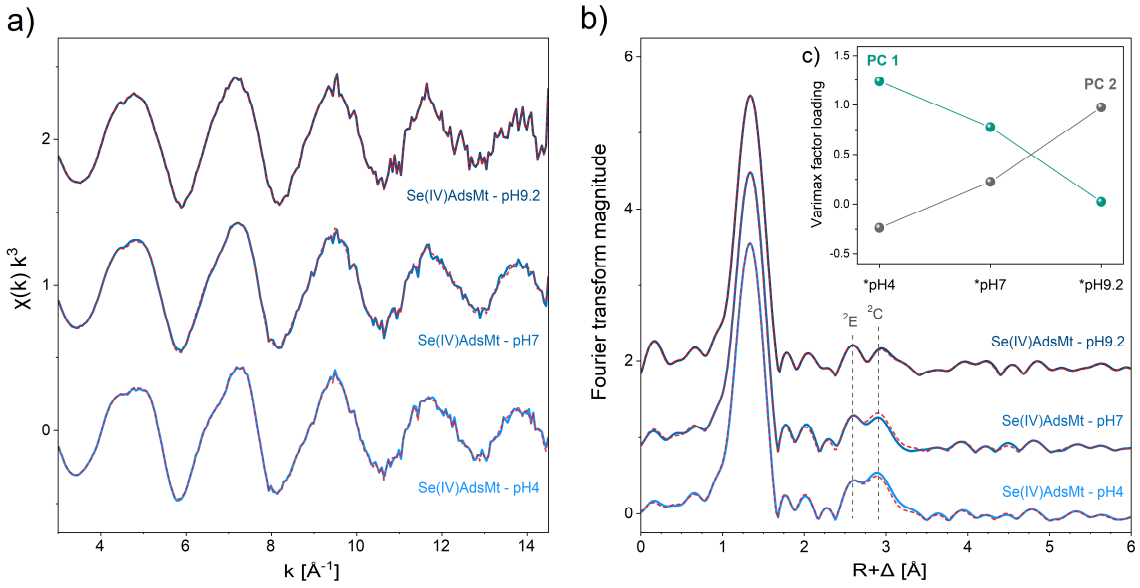

Fig. 6: (a & b) Se K-edge EXAFS spectra of magnetite samples from selenite adsorption studies performed at different pH values (blue lines) and their reconstruction by two factors (red lines). (c) Varimax loadings of the two factors.

The dependency of the complexation type from the pH value can basically be interpreted that increasing pH values and a higher negative surface charge cause a change in the stability and

thus in the prevailing dominance of the selenite adsorption complexes. Under favorable adsorption conditions, the affinity of selenite oxyanions to form corner-sharing ^{2}C complexes is generally higher than for the edge-sharing ^{2}E complexes, leading to a quantitatively predominant of the ^{2}C complexes over a wide pH range. However, at more alkaline conditions, which are generally unfavorable for selenite adsorption, the ^{2}E complexes become more stable. This effect leads to a significant increase in the proportion of ^{2}E over ^{2}C complexes, although the absolute amount of adsorbed selenite decreases with increasing pH.

4 Conclusion

When redox-sensitive materials are considered to prevent the migration of pollutants, it must be taken into account that the retention properties of these materials can change considerably in natural environments. This study demonstrates that magnetite nanoparticles can effectively remediate selenite and selenate contaminated wastewaters even if they are oxidized. However, the retention requires suitable hydrochemical conditions, which mainly concern the prevailing pH and the corresponding selenium speciation. While retention of selenate only takes place at acidic conditions, selenite is immobilized over a large pH range. No reduction processes were involved in the selenium immobilization. The specific retention mechanism are attributable to the formation of surface adsorption complexes. A mixture of mononuclear edge-sharing (^{2}E) and binuclear corner-sharing (^{2}C) inner-sphere complexes in case of selenite and most likely outer-sphere surface complexes in case of selenate. It was found that both types of inner-sphere selenite complexes have different affinities and stabilities depending on the solution pH.

Regarding the assessment of the remediation efficiencies of oxidized magnetite, the results show that the mechanisms of selenate and selenate adsorption are comparable to the findings from previous adsorption studies on pure maghemite. Accordingly, in systems where no reduction takes place, partially oxidized magnetite nanoparticles can approximately be considered as a maghemite-like adsorbent phase. These findings help to better understand the retention behavior of selenium oxyanions in contact with nanoparticulate magnetite/maghemite phases under oxic conditions and could be used in modeling the migration of selenium oxyanions in subsurface environments.

Conflicts of interest

There are no conflicts of interest to declare.

Acknowledgements

This work is part of the *IMMORAD* project, funded by the German Federal Ministry for Education and Research (BMBF) under grant No. 02NUK019B. Additional financial support was provided by the Graduate School for Climate and Environment (GRACE) at KIT. The authors would like to thank Dr. Peter Weidler and Volker Zibat for BET and SEM analyses. We also thank Dr. Utz Kramar and Claudia Mößner for their help with XRF and ICP-MS analyses. The ESRF and the team of the Rossendorf Beamline (BM 20) are gratefully acknowledged for the provision of beam time and their support during the XAFS measurements.

References

Ankudinov A. L. and Rehr J. J. (1997) Relativistic calculations of spin-dependent x-ray-absorption spectra. *Phys. Rev. B* **56**, 1712–1715.

Bingham P. A., Connelly A. J., Cassingham N. J. and Hyatt N. C. (2011) Oxidation state and local environment of selenium in alkali borosilicate glasses for radioactive waste immobilisation. *J. Non. Cryst. Solids* **357**, 2726–2734.

Börsig N., Scheinost A. C., Shaw S., Schild D. and Neumann T. (2018) Retention and multiphase transformation of selenium oxyanions during the formation of magnetite via iron(ii) hydroxide and green rust. *Dalt. Trans.* **47**, 11002–11015.

Börsig N., Scheinost A. C., Shaw S., Schild D. and Neumann T. (2017) Uptake mechanisms of selenium oxyanions during the ferrihydrite-hematite recrystallization. *Geochim. Cosmochim. Acta* **206**, 236–253.

De Cannière P., Maes A., Williams S., Bruggeman C., Beauwens T., Maes N. and Cowper M. (2010) *Behaviour of Selenium in Boom Clay. External Report of the Belgian Nuclear Research Centre*., SCK•CEN-ER-120, Mol, BEL.

Chan Y. T., Kuan W. H., Chen T. Y. and Wang M. K. (2009) Adsorption mechanism of selenate and selenite on the binary oxide systems. *Water Res.* **43**, 4412–4420.

Chowdhury S. R. and Yanful E. K. (2010) Arsenic and chromium removal by mixed magnetite-maghemite nanoparticles and the effect of phosphate on removal. *J. Environ. Manage.* **91**, 2238–2247.

Cornell R. M. and Schwertmann U. (2003) *The iron oxydes: Structure, Properties, Reactions, Occurences and Uses*. 2nd ed., Wiley-VCH, Weinheim, Germany.

Dhillon K. S. and Dhillon S. K. (2003) Distribution and management of seleniferous soils. *Adv. Agron.* **79**, 119–184.

Duc M., Lefèvre G., Fédoroff M., Jeanjean J., Rouchaud J. C., Monteil-Rivera F., Dumonceau J. and Milonjic S. (2003) Sorption of selenium anionic species on apatites and iron oxides from aqueous solutions. *J. Environ. Radioact.* **70**, 61–72.

Fernández-Martínez A. and Charlet L. (2009) Selenium environmental cycling and bioavailability: A structural chemist point of view. *Rev. Environ. Sci. Biotechnol.* **8**, 81–110.

Frechou C., Aguerre S., Degros J. P., Kerlau G. and Grangeon T. (2007) Improvement of a radiochemical separation for selenium 79: Applications to effluents and nuclear wastes. *Talanta* **72**, 1166–1171.

Fukushi K. and Sverjensky D. A. (2007) A surface complexation model for sulfate and selenate on iron oxides consistent with spectroscopic and theoretical molecular evidence. *Geochim. Cosmochim. Acta* **71**, 1–24.

Génin J.-M. R., Ruby C., Géhin A. and Refait P. (2006) Synthesis of green rusts by oxidation of $Fe(OH)_2$, their products of oxidation and reduction of ferric oxyhydroxides; Eh-pH Pourbaix diagrams. *Comptes Rendus Geosci.* **338**, 433–446.

Gorski C. A. and Scherer M. M. (2010) Determination of nanoparticulate magnetite stoichiometry by Mössbauer spectroscopy, acidic dissolution, and powder X-ray diffraction: A critical review. *Am. Mineral.* **95**, 1017–1026.

Hawthorne F. C. (1984) The crystal structure of mandarinoite, $Fe^{3+}{}_2Se_3O_9 \cdot 6H_2O$. *Can. Mineral.* **22**, 475–480.

Hayes K. F., Roe A. L., Brown G. E., Hodgson K. O., Leckie J. O. and Parks G. A. (1987) In Situ X-ray Absorption Study of Surface Complexes: Selenium Oxyanions on α-FeOOH. *Science (80-.).* **238**, 783–786.

He Y. T. and Traina S. J. (2005) Cr(VI) reduction and immobilization by magnetite under alkaline pH conditions: The role of passivation. *Environ. Sci. Technol.* **39**, 4499–4504.

Hiemstra T., Rietra R. P. J. J. and Van Riemsdijk W. H. (2007) Surface Complexation of Selenite on Goethite: MO/DFT Geometry and Charge Distribution. *Croat. Chem. Acta* **80**, 313–324.

Horst M. F., Lassalle V. and Ferreira M. L. (2015) Nanosized magnetite in low cost materials for remediation of water polluted with toxic metals, azo- and antraquinonic dyes. *Front. Environ. Sci. Eng*. **9**, 746–769.

Hu J. D., Zevi Y., Kou X. M., Xiao J., Wang X. J. and Jin Y. (2010) Effect of dissolved organic matter on the stability of magnetite nanoparticles under different pH and ionic strength conditions. *Sci. Total Environ.* **408**, 3477–3489.

Iwatsuki M. and Fukasawa T. (1993) Nondestructive and Complete Analysis of Magnetite-Maghemite Solid Solutions by a Combined X-Ray Diffraction/Fluorescence Method. *Anal. Sci.* **9**, 95–98.

Jönsson J. and Sherman D. M. (2008) Sorption of As(III) and As(V) to siderite, green rust (fougerite) and magnetite: Implications for arsenic release in anoxic groundwaters. *Chem. Geol.* **255**, 173–181.

Jordan N., Lomenech C., Marmier N., Giffaut E. and Ehrhardt J.-J. (2009) Sorption of selenium(IV) onto magnetite in the presence of silicic acid. *J. Colloid Interface Sci.* **329**, 17–23.

Jordan N., Ritter A., Foerstendorf H., Scheinost A. C., Weiß S., Heim K., Grenzer J., Mücklich A. and Reuther H. (2013) Adsorption mechanism of selenium(VI) onto maghemite. *Geochim. Cosmochim. Acta* **103**, 63–75.

Jordan N., Ritter A., Scheinost A. C., Weiss S., Schild D. and Hübner R. (2014) Selenium(IV) uptake by maghemite (γ-Fe_2O_3). *Environ. Sci. Technol.* **48**, 1665–1674.

Khan U. S., Amanullah, Manan A., Khan N., Mahmood A. and Rahim A. (2015) Transformation mechanism of magnetite nanoparticles. *Mater. Sci. Pol.* **33**, 278–285.

Kim S. S., Min J. H., Lee J. K., Baik M. H., Choi J.-W. and Shin H. S. (2012) Effects of pH and anions on the sorption of selenium ions onto magnetite. *J. Environ. Radioact.* **104**, 1–6.

Kirsch R., Scheinost A. C., Rossberg A., Banerjee D. and Charlet L. (2008) Reduction of antimony by nano-particulate magnetite and mackinawite. *Mineral. Mag.* **72**, 185–189.

Kuhn L. T., Bojesen A., Timmermann L., Nielsen M. M. and Mørup S. (2002) Structural and magnetic properties of core-shell iron-iron oxide nanoparticles. *J. Phys. Condens. Matter* **14**, 13551–13567.

Kuppusamy S., Palanisami T., Megharaj M., Venkateswarlu K. and Naidu R. (2016) In-Situ Remediation Approaches for the Management of Contaminated Sites: A Comprehensive Overview. In *Reviews of Environmental Contamination and Toxicology Volume 236* (ed. P. de Voogt). Springer International Publishing, Cham. pp. 1–115.

Latta D. E., Gorski C. A., Boyanov M. I., O'Loughlin E. J., Kemner K. M. and Scherer M. M. (2012) Influence of Magnetite Stoichiometry on U^{VI} reduction. *Environ. Sci. Technol.* **46**, 778–786.

Lemly A. D. (2004) Aquatic selenium pollution is a global environmental safety issue. *Ecotoxicol. Environ. Saf.* **59**, 44–56.

Lenz M. and Lens P. N. L. (2009) The essential toxin: The changing perception of selenium in environmental sciences. *Sci. Total Environ.* **407**, 3620–3633.

Li Z., Liu M., Chen L. K. and Li G. Z. (2017) Combined Toxicity of an Environmental Remediation Residue, Magnetite Fe_3O_4 Nanoparticles/Cr(VI) Adduct. *Biomed. Environ. Sci.* **30**, 783–791.

Liu A., Liu J., Pan B. and Zhang W. X. (2014) Formation of lepidocrocite (γ-FeOOH) from oxidation of nanoscale zero-valent iron (nZVI) in oxygenated water. *RSC Adv.* **4**, 57377–57382.

Liu C. H., Chuang Y. H., Chen T. Y., Tian Y., Li H., Wang M. K. and Zhang W. (2015) Mechanism of Arsenic Adsorption on Magnetite Nanoparticles from Water: Thermodynamic and Spectroscopic Studies. *Environ. Sci. Technol.* **49**, 7726–7734.

Loyo R. L. de A., Nikitenko S. I., Scheinost A. C. and Simonoff M. (2008) Immobilization of selenite on Fe_3O_4 and Fe/Fe_3C ultrasmall particles. *Environ. Sci. Technol.* **42**, 2451–2456.

Manceau A. and Charlet L. (1994) The Mechanism of Selenate Adsorption on Goethite and Hydrous Ferric Oxide. *J. Colloid Interface Sci.* **168**, 87–93.

Martínez M., Giménez J., de Pablo J., Rovira M. and Duro L. (2006) Sorption of selenium(IV) and selenium(VI) onto magnetite. *Appl. Surf. Sci.* **252**, 3767–3773.

Milonjić S. K., Kopečni M. M. and Ilić Z. E. (1983) The point of zero charge and adsorption properties of natural magnetite. *J. Radioanal. Chem.* **78**, 15–24.

Missana T., Alonso U., Scheinost A. C., Granizo N. and García-Gutiérrez M. (2009) Selenite retention by nanocrystalline magnetite: Role of adsorption, reduction and dissolution/co-precipitation processes. *Geochim. Cosmochim. Acta* **73**, 6205–6217.

Morin G., Ona-Nguema G., Wang Y., Menguy N., Juillot F., Proux O., Guyot F., Calas G. and Brown G. E. (2008) Extended X-ray absorption fine structure analysis of arsenite and arsenate adsorption on maghemite. *Environ. Sci. Technol.* **42**, 2361–2366.

Mu Y., Jia F., Ai Z. and Zhang L. (2017) Iron oxide shell mediated environmental remediation properties of nano zero-valent iron. *Environ. Sci. Nano* **4**, 27–45.

Munier-Lamy C., Deneux-Mustin S., Mustin C., Merlet D., Berthelin J. and Leyval C. (2007) Selenium bioavailability and uptake as affected by four different plants in a loamy clay soil with particular attention to mycorrhizae inoculated ryegrass. *J. Environ. Radioact.* **97**, 148–158.

Nakamaru Y. M. and Altansuvd J. (2014) Speciation and bioavailability of selenium and antimony in non-flooded and wetland soils: A review. *Chemosphere* **111**, 366–371.

Navarathna C. M., Karunanayake A. G., Gunatilake S. R., Pittman C. U., Perez F., Mohan D. and Mlsna T. (2019) Removal of Arsenic(III) from water using magnetite precipitated onto Douglas fir biochar. *J. Environ. Manage.* **250**, 109429.

Peak D. and Sparks D. L. (2002) Mechanisms of selenate adsorption on iron oxides and hydroxides. *Environ. Sci. Technol.* **36**, 1460–1466.

Rebodos R. L. and Vikesland P. J. (2010) Effects of oxidation on the magnetization of nanoparticulate

magnetite. *Langmuir* **26**, 16745–16753.

Ressler T. (1998) WinXAS: a program for X-ray absorption spectroscopy data analysis under MS-Windows. *J. Synchrotron Radiat.* **5**, 118–122.

Rietra R. P. J. J., Hiemstra T. and van Riemsdijk W. H. (2001) Comparison of Selenate and Sulfate Adsorption on Goethite. *J. Colloid Interface Sci.* **240**, 384–390.

Rossberg A., Reich T. and Bernhard G. (2003) Complexation of uranium(VI) with protocatechuic acid-application of iterative transformation factor analysis to EXAFS spectroscopy. *Anal. Bioanal. Chem.* **376**, 631–638.

Rovira M., Giménez J., Martínez M., Martínez-Lladó X., de Pablo J., Martí V. and Duro L. (2008) Sorption of selenium(IV) and selenium(VI) onto natural iron oxides: Goethite and hematite. *J. Hazard. Mater.* **150**, 279–284.

Salah S. and Wang L. (2014) *Speciation and solubility calculations for waste relevant radionuclides in Boom Clay. External Report of the Belgian Nuclear Research Centre.*, SCK•CEN-ER-198, Mol, BEL.

Salazar Camacho C. A. and Villalobos Peñalosa M. (2017) Characterization and surface reactivity of natural and synthetic magnetites: II. adsorption of Pb(II) and Zn(II). *Rev. Int. Contam. Ambient.* **33**, 165–176.

Scheinost A. C. and Charlet L. (2008) Selenite reduction by mackinawite, magnetite and siderite: XAS characterization of nanosized redox products. *Environ. Sci. Technol.* **42**, 1984–1989.

Scheinost A. C., Kirsch R., Banerjee D., Fernandez-Martinez A., Zaenker H., Funke H. and Charlet L. (2008) X-ray absorption and photoelectron spectroscopy investigation of selenite reduction by FeII-bearing minerals. *J. Contam. Hydrol.* **102**, 228–245.

Schwaminger S. P., Bauer D., Fraga-García P., Wagner F. E. and Berensmeier S. (2017) Oxidation of magnetite nanoparticles: impact on surface and crystal properties. *CrystEngComm* **19**, 246–255.

Séby F., Potin-Gautier M., Giffaut E., Borge G. and Donard O. F. X. (2001) A critical review of thermodynamic data for selenium species at 25°C. *Chem. Geol.* **171**, 173–194.

Sharifi Dehsari H., Ksenofontov V., Möller A., Jakob G. and Asadi K. (2018) Determining Magnetite/Maghemite Composition and Core-Shell Nanostructure from Magnetization Curve for Iron Oxide Nanoparticles. *J. Phys. Chem. C* **122**, 28292–28301.

Signorini L., Pasquini L., Savini L., Carboni R., Boscherini F., Bonetti E., Giglia A., Pedio M., Mahne N., Mahne N., Nannarone S. and Nannarone S. (2003) Size-dependent oxidation in iron/iron oxide core-shell nanoparticles. *Phys. Rev. B - Condens. Matter Mater. Phys.* **68**, 1–8.

Su C. and Suarez D. L. (2000) Selenate and Selenite Sorption on Iron Oxides. *Soil Sci. Soc. Am. J.* **64**, 101–111.

Tan L. C., Nancharaiah Y. V., van Hullebusch E. D. and Lens P. N. L. (2016) Selenium: environmental significance, pollution, and biological treatment technologies. *Biotechnol. Adv.* **34**, 886–907.

Usman M., Byrne J. M., Chaudhary A., Orsetti S., Hanna K., Ruby C., Kappler A. and Haderlein S. B. (2018) Magnetite and Green Rust: Synthesis, Properties, and Environmental Applications of Mixed-Valent Iron Minerals. *Chem. Rev.* **118**, 3251–3304.

Wang Y., Morin G., Ona-Nguema G., Juillot F., Calas G. and Brown G. E. (2011) Distinctive arsenic(V) trapping modes by magnetite nanoparticles induced by different sorption processes. *Environ. Sci. Technol.* **45**, 7258–7266.

Wang Y., Morin G., Ona-Nguema G., Menguy N., Juillot F., Aubry E., Guyot F., Calas G. and Brown G. E. (2008) Arsenite sorption at the magnetite-water interface during aqueous precipitation of magnetite: EXAFS evidence for a new arsenite surface complex. *Geochim. Cosmochim. Acta* **72**,

2573–2586.

Weidner E. and Ciesielczyk F. (2019) Removal of hazardous oxyanions from the environment using metal-oxide-based materials. *Materials (Basel).* **16**.

Wilkin R. T., Su C., Ford R. G. and Paul C. J. (2005) Chromium-removal processes during groundwater remediation by a zerovalent iron permeable reactive barrier. *Environ. Sci. Technol.* **39**, 4599–4605.

Wylie E. M., Olive D. T. and Powell B. A. (2016) Effects of Titanium Doping in Titanomagnetite on Neptunium Sorption and Speciation. *Environ. Sci. Technol.* **50**, 1853–1858.

Zhang M., Pan G., Zhao D. and He G. (2011) XAFS study of starch-stabilized magnetite nanoparticles and surface speciation of arsenate. *Environ. Pollut.* **159**, 3509–3514.